PAPER

Electron collisions with ArH^+ molecular ions: highly excited vibrational states and dissociative excitation

To cite this article: E Djuissi *et al* 2022 *Plasma Sources Sci. Technol.* **31** 114012

IOP Publishing Plasma Sources Science and Technology
Plasma Sources Sci. Technol. **31** (2022) 114012 (13pp) https://doi.org/10.1088/1361-6595/aca4f3

Electron collisions with ArH^+ molecular ions: highly excited vibrational states and dissociative excitation

E Djuissi[1], A Bultel[2], J Tennyson[1,3], I F Schneider[1,4] and V Laporta[5,*]

[1] Laboratoire Ondes et Milieux Complexes, UMR6294-CNRS–Université Le Havre Normandie, 76058 Le Havre, France
[2] Laboratoire CORIA, UMR6614-CNRS–Université de Rouen Normandie, 76801 Saint-Etienne de Rouvray, France
[3] Department of Physics and Astronomy, University College London, WC1E 6BT London, United Kingdom
[4] Laboratoire Aimé-Cotton, CNRS−Université Paris-Sud−ENS Cachan−Université Paris-Saclay, 91405 Orsay, France
[5] Istituto per la Scienza e Tecnologia dei Plasmi, CNR, 70125 Bari, Italy

E-mail: vincenzo.laporta@istp.cnr.it

Received 10 July 2022, revised 11 November 2022
Accepted for publication 22 November 2022
Published 6 December 2022

Abstract

A theoretical investigation of dissociative recombination and dissociative excitation processes involving electron collisions with the argonium ion (ArH^+) at energies up to 7 eV is presented. Curves and couplings obtained using R-matrix calculations are used to provide the input for molecular dynamics calculations based on the multichannel quantum defect theory. A full set of vibrationally resolved cross sections and rate coefficients is presented for the kinetic modeling of argon-containing non-equilibrium plasma.

Keywords: molecular dynamics, plasma, ArH^+

(Some figures may appear in colour only in the online journal)

1. Introduction

Collisions of electrons with the argonium molecular ion (ArH^+) contribute to the kinetics in numerous natural and industrial cold ionized media. From the technological point of view, ArH^+ is involved in low pressure argon-hydrogen containing plasma, such as those used for etching and cleaning applications. Particularly interesting is its use for cleaning of the HL-1 tokamak wall based on its interaction with a radiofrequency plasma [1]. Argon is preferred to other rare gases for cleaning because of the greater production of its hydride ion which leads to higher efficiency cleaning processes [2]. Argonium is also involved in the surface treatments such as plasma sprays used in aeronautics, gas turbines and automotive fields [3] or in the control of the surface properties of polymers [4]. Conversely, rare-gas hydride ions are also of interest for metrology applications. Indeed, ArH^+ transitions will be used as frequency standards in the terahertz region when precise locking of oscillators is required in quantum cascade lasers or resonant tunnel diodes [5]. Within the framework of metrology, ArH^+ plays a significant role in the analysis performed by inductively coupled plasma mass spectrometry [6].

In natural systems, ArH^+ was recently detected in the Crab Nebula using the Herschel Space Observatory [7] which has resulted in studies of its interstellar medium chemistry [8].

ArH^+ molecular ion is easily formed when argon and hydrogen react with each other and it plays a significant role in

* Author to whom any correspondence should be addressed.

the chemistry at temperatures lower than 3 eV [9]. The formation processes:

$$Ar^+ + H_2 \rightarrow ArH^+ + H, \quad (1)$$

$$Ar + H_2^+ \rightarrow ArH^+ + H, \quad (2)$$

are much more efficient [10] than direct charge exchange:

$$Ar^+ + H_2 \rightarrow Ar + H_2^+. \quad (3)$$

Following reactions (1) and (2), the charge is redistributed to different species, which can lead to modification of the ambipolar diffusion processes. In addition, the formation of ArH^+ opens a channel which can lead to the production of the H_3^+ ion via argon [11],

$$ArH^+ + H_2 \rightarrow H_3^+ + Ar, \quad (4)$$

whose rate coefficient is around a half of the rate coefficient characterizing the main channel,

$$H_2^+ + H_2 \rightarrow H_3^+ + H, \quad (5)$$

in low pressure pure hydrogen plasmas [12]. An assessment of ArH^+ density is therefore important in non-equilibrium conditions.

The above reactions occur, principally, in low pressure inductively coupled plasma in supersonic expansions [13] such as those used for plasma remote deposition. In other recombining plasma, such as plasma arcs at low pressure, dissociative recombination (DR) of ArH^+ is the main source of hydrogen atoms in excited states [14]. Therefore departure from equilibrium can only be modeled by including the behavior of ArH^+.

In spite of its importance, little experimental [15–19] or theoretical information exists for ArH^+. To provide data for astrochemistry modeling, Abdoulanziz *et al* [20] performed calculations using a multichannel quantum defect theory (MQDT) approach [21, 22] and the R-matrix method [23, 24] which provided cross sections and rate coefficients for DR and vibrational excitation/de-excitation (VE/VdE) processes at low energy [7, 25]:

$$e(\varepsilon) + ArH^+(X, v_i^+) \rightarrow ArH^*, ArH^{**} \rightarrow Ar + H, \quad (DR) \quad (6)$$

$$e(\varepsilon) + ArH^+(X, v_i^+) \rightarrow ArH^*, ArH^{**} \rightarrow e(\varepsilon') + ArH^+(X, v_f^+). \quad (VE/VdE) \quad (7)$$

Here v_i^+ and v_f^+ represent the initial and the final vibrational quantum numbers of the target, respectively; ε is the incident electron energy, and ArH^*, ArH^{**} stand for the intermediate bound Rydberg states and for the resonant dissociative states of the neutral molecule, respectively.

However, the data presented by Abdoulanziz *et al* [20] are less accurate for highly excited vibrational levels—$v_i^+ > 2$—and for energies of the electron above the dissociation threshold of the target ion, where dissociative excitation (DE) competes the other collisional processes. The goal of the present work is to continue the calculations initiated by Abdoulanziz *et al* [20] by including in our theoretical approach all the relevant dissociative states whose potential energy curves (PECs) are situated below the PEC of the lowest excited state of the ion. For energies of the incident electron for which the total energy of the system is higher than the dissociation limit of the ground electronic state of the ArH^+, we also take into account the vibrational continuum. This approach allows us to quantify the DE process:

$$e(\varepsilon) + ArH^+(X, v_i^+) \rightarrow ArH^{**} \rightarrow Ar^+(^2P_{3/2}) + H(n = 1) + e, \quad (DE) \quad (8)$$

and its effect in the competition with the processes (6) and (7). On the other hand, this improved approach is by far more appropriate than the previous one for the modeling of the reactive collisions of electron with the ions in highly excited vibrational states.

This paper is organized as follows: in section 2 we present the molecular structure data used in our model. Section 3 gives a brief description of the theoretical approach to the quantum dynamics governing the processes (6)–(8). The DR, VE, VdE and DE cross sections and rate coefficients are given and discussed in section 4. The paper ends with our conclusions.

2. Molecular structure data

The study of molecular quantum dynamics relies on the determination of appropriate molecular structure data. In the case of electron-molecular cation scattering, these data are essentially represented by: (a) the PECs U^+ for the target ArH^+ and $U_{d,n}^{\Omega}$ for the neutral resonant dissociative states ArH^{**}, n being the principal quantum number with respect to the lowest excited state of the ion ArH^+ (b $^3\Pi$), (b) the quantum defect μ_{Ryd}^{Ω} characterizing the Rydberg series of ArH^* and (c) the electronic couplings $V_{d,n}^{\Omega}(R)$ between the n resonant dissociative ($ArH^{**} \rightarrow Ar + H$) states and the ionization continuum ($e^- + ArH^+$). For the current $e^- + ArH^+$ system, three symmetries—labeled by Ω—are considered: $^2\Sigma^+$, $^2\Pi$, and $^2\Delta$. Our previous study [20] employed the *ab initio* R-matrix method [23], using the UKRMol package [24], to characterize six low-lying resonant states. Since the aim of the present paper is to extend the approach used by Abdoulanziz *et al* [20] to the electron impact reactivity of highly excited ions and to the study of the DE, we calculated seven more resonant states—three for the $^2\Sigma^+$ symmetry, three for the $^2\Pi$ symmetry and one of $^2\Delta$ symmetry—giving a total of 13 *ab-initio* resonant states. These states span energies up to 7 eV, which allows the dissociation region to be correctly taken into account.

To fill the gap between the *ab-initio* resonance states and the first electronic excited state of ArH^+, a Rydberg scaling-law [26] was used for each symmetry Ω to generate further approximate resonance PECs. This scaling-law is based on the convergence of the quantum defect μ_n^{Ω}—with respect to the increase in the principal quantum number n of the resonant state—to its value at the ionization threshold.

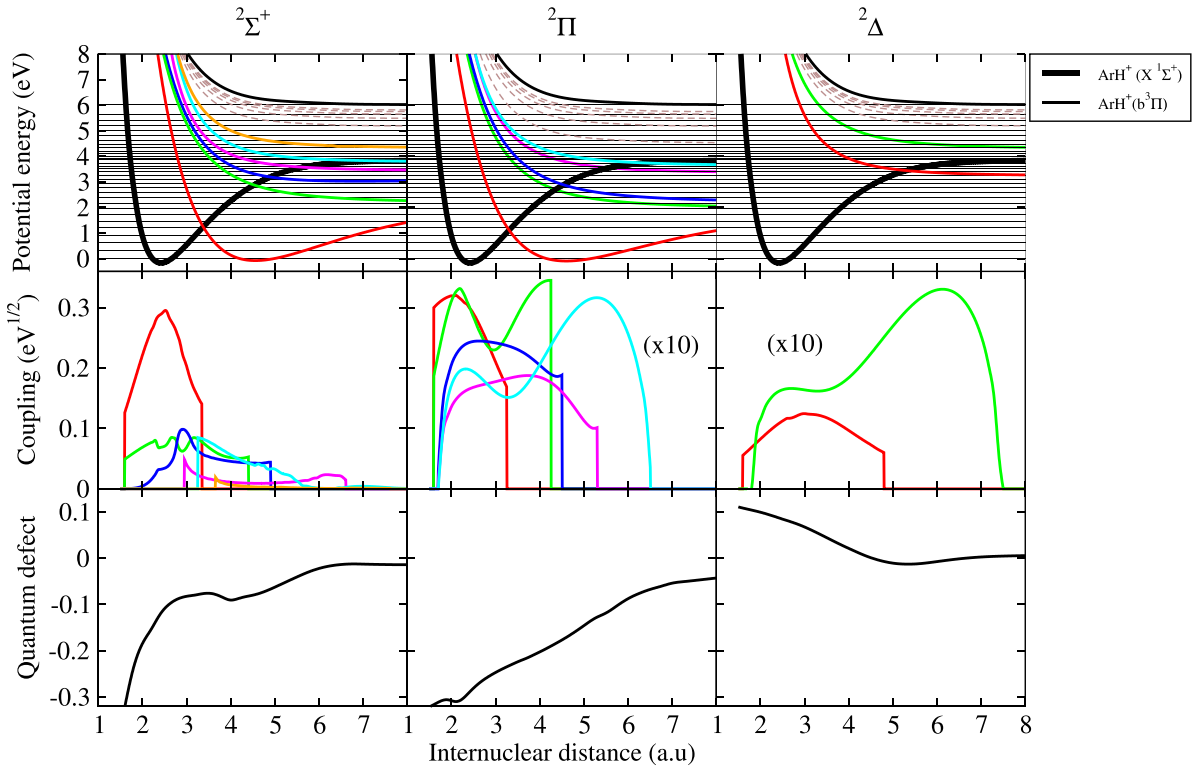

Figure 1. Summary of the molecular data used in the calculations for symmetries, Ω, equal to $^2\Sigma^+$, $^2\Pi$ and $^2\Delta$. Top row: potential energy curves (PECs). The solid thick black curves are the PECs of the ArH^+ ion. Solid colored curves represent the resonant states of ArH obtained using the R-matrix method; dashed curve were generated using the scaling law. The thin black horizontal lines are the vibrational levels of the ground state of the ion. Those situated above the asymptotic limit of the PEC of the ground state correspond to the discretization of the continuum, invoked at the end of section 2. Only a quarter of them are drawn, in order to keep the figure readable. Middle row: electronic couplings for R-matrix states only. To aid visualization, the $^2\Pi$ and $^2\Delta$ symmetry coupling curves are scaled by a factor 10. Bottom row: quantum defects $\mu^{\Omega}_{\rm Ryd}$ of the mono-excited Rydberg series.

Labeling the principal quantum number of the most excited dissociative states of symmetry Ω produced *ab initio* as n_h^{Ω}—the sixth state for the $^2\Sigma^+$ symmetry, the fifth for the $^2\Pi$ one and the second for the $^2\Delta$ one—and setting $n^{\Omega}_{\rm min} = n_h^{\Omega} + 1$, we generated the approximate PECs for the further excited states with principal quantum numbers in the range $[n^{\Omega}_{\rm min}, n^{\Omega}_{\rm max}]$ by applying the formula:

$$U^{\Omega}_{d,n}(R) = U^{+*}(R) - \frac{\rm Ryd}{[n-\mu^{\Omega}_{n_h^{\Omega}}(R)]^2}\,, \qquad n = n^{\Omega}_{\rm min}, \ldots n^{\Omega}_{\rm max}, \tag{9}$$

where U^{+*} represents the PEC of the lowest excited electronic state of the ion, $n^{\Omega}_{\rm min}$ is 7, 6 and 3 for the symmetries $^2\Sigma^+$, $^2\Pi$, and $^2\Delta$, respectively. After checking convergence, we set $n^{\Omega}_{\rm max} = n^{\Omega}_{\rm min} + 4$ for each symmetry so that in total we have 25 resonant states in our model. The corresponding resonance widths are given by:

$$\Gamma^{\Omega}_{d,n}(R) = \frac{1}{[n-\mu^{\Omega}_{n_h^{\Omega}}(R)]^3}\bar{\Gamma}^{\Omega}_{d}(R)\,, \qquad n = n^{\Omega}_{\rm min}, \ldots n^{\Omega}_{\rm max}\,, \tag{10}$$

where $\bar{\Gamma}^{\Omega}_{d}(R)$ is given by :

$$\bar{\Gamma}^{\Omega}_{d}(R) = \Gamma_{d,n_h^{\Omega}}(R)[n_h^{\Omega} - \mu^{\Omega}_{n_h^{\Omega}}(R)]^3\,. \tag{11}$$

The electronic couplings are calculated using:

$$V^{\Omega}_{d,n} = \sqrt{\frac{\Gamma^{\Omega}_{d,n}}{2\pi}}\,, \qquad n = n^{\Omega}_{\rm min}\ \ldots n^{\Omega}_{\rm max}\,. \tag{12}$$

Figure 1 summarizes the molecular structure data used in the calculations, while table 1 lists the ArH^+ vibrational states considered along with spectroscopic parameters, and table 2 shows the asymptotic limits of the ArH^{**} resonant states with products and the relevant symmetries. The vibrational levels and the pseudo-continuum part of the ArH^+ spectrum were computed using the spectral representation method [27].

3. MQDT approach

3.1. Reactive processes below the ion dissociation threshold

Quantum dynamics calculations were performed in the framework of the MQDT approach [21, 29–35]. The MQDT methodology has already been applied in previous work [22, 34–38], where full theoretical details can be found. Consequently, here we present the main features only. As we neglect rotational couplings, meaning that Λ-mixing is neglected, the approach described below is applied separately for each

Table 1. Molecular constants (reduced mass, equilibrium distance and dissociating energies) for $^{40}ArH^+$ in its ground electronic state and the energies of the corresponding vibrational levels. Comparison with the experimental data of Hotop *et al* [28] is given in parentheses.

μ (a.u.)	1791.94		
R_{eq} (a.u.)	2.419 (2.419)		
D_e (eV)	4.039 (4.025)		
D_0 (eV)	3.8725		
v^+	ϵ_{v^+} (eV)	v^+	ϵ_{v^+} (eV)
0	0.000	12	2.949
1	0.321	13	3.110
2	0.627	14	3.258
3	0.919	15	3.393
4	1.197	16	3.513
5	1.461	17	3.617
6	1.712	18	3.703
7	1.949	19	3.770
8	2.174	20	3.817
9	2.387	21	3.846
10	2.587	22	3.861
11	2.774		

Table 2. Asymptotic limits of the ArH^{**} resonant states relevant for low-energy impact collisions. The energy are given with respect to the $v^+ = 0$ vibrational level of ArH^+.

Channel	Energies (eV)	Symmetries
$Ar(^2P_{3/2}\ 4s) + H(n = 1)$	1.822	$1\,^2\Pi$
$Ar(^2P_{1/2}\ 4s) + H(n = 1)$	2.102	$1\,^2\Sigma^+, 2\,^2\Pi$
$Ar(^1S) + H(n = 3)$	2.369	$2\,^2\Sigma^+, 3\,^2\Pi,$
$Ar(^2P_{3/2}\ 4p) + H(n = 1)$	3.181	$3\,^2\Sigma^+$
$Ar(^1S) + H(n = 5)$	3.329	$1\,^2\Delta, 4\,^2\Pi$
$Ar(^2P_{1/2}\ 4p) + H(n = 1)$	3.576	$4\,^2\Sigma^+$
$Ar(^1S) + H(n = 7)$	3.595	$5\,^2\Pi$
$Ar(^2P_{1/2}\ 4p) + H(n = 1)$	3.754	$5\,^2\Sigma^+$
$Ar(^2P_{3/2}\ 5s) + H(n = 1)$	4.337	$2\,^2\Delta, 6\,^2\Sigma^+$

symmetry, Ω. To simplify the notation, we do not specify the index Ω, unless necessary.

Basically, in the MQDT approach for electron-molecular cation scattering, one has to build-up the reaction matrix $\boldsymbol{\mathcal{K}}$ which satisfies the Lippmann–Schwinger equation [39]:

$$\boldsymbol{\mathcal{K}} = \boldsymbol{\mathcal{V}} + \boldsymbol{\mathcal{V}} \frac{1}{E - \boldsymbol{H_0}} \boldsymbol{\mathcal{K}}, \tag{13}$$

where $\boldsymbol{H_0}$ is the zero-order Hamiltonian of the system, E is the total energy and $\boldsymbol{\mathcal{V}}$ is the interaction matrix whose non-vanishing elements depend on the electronic couplings $V^{\Omega}_{d,n}$:

$$\mathcal{V}^{\Omega}_{d,n}(E) = \langle \chi^{\Omega}_{d,n}(E) | V^{\Omega}_{d,n} | \chi_{v^+} \rangle, \tag{14}$$

where $\chi^{\Omega}_{d,n}$ and χ_{v^+} are the nuclear wave function corresponding to the resonant states $U^{\Omega}_{d,n}(R)$ and to the target ion $U^+(R)$, respectively. In the following, we consider the second-order perturbation theory solution of equation (13) with the $\boldsymbol{\mathcal{K}}$ matrix on its right-hand side replaced by the $\boldsymbol{\mathcal{V}}$ matrix.

Short-range eigenchannels functions are obtained by diagonalizing the reaction matrix $\boldsymbol{\mathcal{K}}$:

$$\boldsymbol{\mathcal{K}}\boldsymbol{\mathcal{U}} = -\frac{1}{\pi} \tan(\boldsymbol{\eta}) \boldsymbol{\mathcal{U}}, \tag{15}$$

via the phase shifts $\boldsymbol{\eta}$ and the eigenfunctions $\boldsymbol{\mathcal{U}}$. Conversely, to obtain long-range solutions, where the Born–Oppenheimer representation is no longer valid and Λ, for each symmetry Ω, cannot be treated as a good quantum number, a frame transformation is performed linking the $\boldsymbol{\mathcal{U}}$ basis set to the asymptotic channels v^+ and d via the projection matrices $\boldsymbol{\mathcal{C}}$ and $\boldsymbol{\mathcal{S}}$:

$$\mathcal{C}_{v^+:\Omega\alpha} = \sum_{v} \mathcal{U}^{\Omega}_{v:\alpha} \langle \chi_{v^+} | (\cos(\pi \mu^{\Omega}_{\mathrm{Ryd}} + \eta^{\Omega}_{\alpha}) | \chi^{\Omega}_{v} \rangle, \tag{16}$$

$$\mathcal{C}_{d,n:\Omega\alpha} = \mathcal{U}^{\Omega}_{d,n:\alpha} \cos(\eta^{\Omega}_{\alpha}). \tag{17}$$

The coefficients of the matrix $\boldsymbol{\mathcal{S}}$ are obtained by replacing cosine by sine in the above formulas. In equation (16), χ^{Ω}_{v} represents the vibrational wave function in a Rydberg state and here we make the approximation $\chi^{\Omega}_{v} \approx \chi_{v^+}$.

From the projection matrices $\boldsymbol{\mathcal{C}}$ and $\boldsymbol{\mathcal{S}}$, the generalized diffusion matrix $\boldsymbol{X}$ can be written:

$$\boldsymbol{X} = \frac{\boldsymbol{\mathcal{C}} + i\boldsymbol{\mathcal{S}}}{\boldsymbol{\mathcal{C}} - i\boldsymbol{\mathcal{S}}} = \begin{pmatrix} X_{\mathrm{oo}} & X_{\mathrm{oc}} \\ X_{\mathrm{co}} & X_{\mathrm{cc}} \end{pmatrix}, \tag{18}$$

where the elements are rearranged in four sub-matrices by considering open (o) and closed (c) channels; the 'physical' scattering matrix $\boldsymbol{S}$ is obtained by elimination of the closed channels:

$$\boldsymbol{S} = X_{\mathrm{oo}} - X_{\mathrm{oc}} \frac{1}{X_{\mathrm{cc}} - \exp(-\mathrm{i}2\pi\nu)} X_{\mathrm{co}}, \tag{19}$$

where $\exp(-\mathrm{i}2\pi\nu)$ represents the matrix with effective quantum number ν_{v^+} associated with the vibrational threshold of the closed ionization channels.

Finally, from the scattering matrix $\boldsymbol{S}$, the cross sections for DR and the vibrational transition processes reads:

$$\sigma_{d \leftarrow v^+_{\mathrm{i}}}(\varepsilon) = \frac{\pi}{4\varepsilon} \sum_{\Omega} \rho^{\Omega} \sum_{n} \left| \boldsymbol{S}^{\Omega}_{d,n:v^+_{\mathrm{i}}} \right|^2, \tag{20}$$

$$\sigma_{v^+_{\mathrm{f}} \leftarrow v^+_{\mathrm{i}}}(\varepsilon) = \frac{\pi}{4\varepsilon} \sum_{\Omega} \rho^{\Omega} \left| \boldsymbol{S}^{\Omega}_{v^+_{\mathrm{f}}:v^+_{\mathrm{i}}} - \delta_{v^+_{\mathrm{f}} v^+_{\mathrm{i}}} \right|^2, \tag{21}$$

where ρ^{Ω} stands for the ratio between the multiplicity of the neutral system and that of the ion.

3.2. Extension of the formalism to the high-energy region: the inclusion of the vibrational continuum

The formalism described in the preceding subsection models the vibrational transitions of the target ion in its ground electronic state, as well as the temporary resonant capture of the electron into Rydberg states with the ion ground state as their core. This is sufficient for low incident electron energies i.e. *below* the dissociation threshold of the ion. For higher energies we use the theoretical approach given by Chakrabarti *et al* [40]. Accordingly, we have to take into account autoionization into states lying in the continuum part of the vibrational spectrum, i.e. the *dissociative excitation*—DE, equation (8).

When this process is included in our approach, the coupling between a given dissociation channel d,n and an ionization one v^+, equation (14), is extended to the continuum part of the vibrational spectrum. Numerically, this is achieved by discretizing the continuum. Instead of doing this by providing a wall at large internuclear distances as done by Chakrabarti *et al* [40], we used a Fourier-grid method [27] relying on the 2500 points which characterize the range of the internuclear distances taken into account. We choose to use the grid method because it gives at the same time, in one calculation, the full vibrational ladder.

The inclusion of DE through the ionization channels associated with the discretized levels from the vibrational continuum of the target increases the dimension of the interaction matrix $\boldsymbol{\mathcal{V}}$ (equation (14)), of the reaction K-matrix $\boldsymbol{\mathcal{K}}$, (equation (13)), of the frame transformation matrices $\boldsymbol{\mathcal{C}}$ (equations (16) and (17)) and of $\boldsymbol{\mathcal{S}}$. Furthermore, the summation on the right-hand side of equation (16) is also extended to the levels from the vibrational continuum. Eventually, the $\boldsymbol{X}$-matrix, the $\boldsymbol{S}$-matrix, the DR cross sections and the VE/VdE ones are built using equations (18)–(21), respectively.

Finally, the DE cross section is computed treating it as simultaneous VE processes from an initial vibrational state v_i^+, to all the energetically-accessible levels of the discretized vibrational continuum of the ion. The cross section is then given by:

$$\sigma^{\Omega}_{\mathrm{DE},\, v_i^+} = \frac{\pi}{4\varepsilon} \sum_{\Omega} \rho^{\Omega} \sum_{v_h^+ < v^+ \leqslant v^+_{\max}(\varepsilon)} |S^{\Omega}_{v^+,\, v_i^+}|^2, \qquad (22)$$

where v_h^+ is the highest *bound* vibrational level supported by the ion PEC, and $v^+_{\max}(\varepsilon)$ is the highest *quasi-continuum* vibrational level situated below the total energy $E = E_{v_i^+} + \varepsilon$ being considered.

4. Results and discussions

Figures 2 and 3 summarize our results. Figure 2 reports the vibrationally-resolved cross sections, summed over all 25 states of the three symmetries. The results are organized in four plots corresponding to the four processes DR equation (6), VE and VdE equation (7) and DE (8) as a function of the incoming electron energy up to 7 eV.

Several features can be noted in the curves. For DR at low energies as the curves show several narrow resonances which result from the capture of the incoming electron into the Rydberg states. Above the dissociation threshold of the ArH^+ ion ground state, marked by the beginning of black vertical lines in the plots, these resonances disappear as our calculations do not consider Rydberg states in the continuum. The VE and VdE processes also show the presence of resonances due to the Rydberg and resonant states at low energy, as for DR.

The DE processes in the so-called discretized vibrational continuum, that is above the threshold to ArH^+ dissociation, all ionization channels are open and the molecular dynamics is driven by the direct mechanism.

For the $v^+ = 0$ vibrational level, comparing the various competitive processes, DR gives the largest cross section. We also note the low-energy enhancement of the cross sections, in particular for the VE and DR processes from highly excited vibrational levels. This effect is due to the low-lying resonant states of ArH^{**} which lie very close to the ground electronic state of ArH^+ (e.g. see solid red curves in the top line of figure 1) for the symmetries $^2\Sigma^+$ and $^2\Pi$. This effect is particularly evident for the $^2\Sigma^+$ because of the very large coupling between ionization channels and dissociation one (see red curve in the first plot, middle line in figure 1).

Finally, the cross sections can be used to provide rates. Figure 3 shows the Maxwellian DR and DE rate coefficients calculated up to a temperature of 15 000 K.

One should notice that the involvement in the calculation of further dissociative states with respect to our previous study has little effect on the rate coefficients corresponding to the ground and to the two lowest vibrationally excited states, as shown in figure 4 for the case of DR. However, the importance of these dissociative states increases notably with the VE of the target.

As for the comparison with the storage ring experiment [15], figure 4 from our previous article Abdoulanziz *et al* [20] does not change significantly, since the DE process is, according to our present figure 3, much slower than DR for $v_i^+ = 0$.

Since the data we produced are meant to be used in collisional-radiative modeling of the cold plasmas, it is important to estimate the accuracy of our calculations.

As concerns our formalism, the main source of inaccuracy—less than 50 % for the cross section, locally, i.e. at some resonance energies—is the use of quantum defects independent of energy. However, this concerns a limited energy range, typically below 0.5 eV—where the position and the amplitude of some of the Rydberg resonances, as those appearing in figure 2, may be under-or over-estimated. Luckily, in terms of thermal rate coefficients, this results in a much lower inaccuracy, of the order of 20%–30%, especially above the dissociation threshold.

However, we critically rely on molecular structure data—PEC's and autoionization widths, as those displayed in figure 1. Their computation, mainly based on the R-matrix theory, is extremely complex, and their inaccuracy may be much larger than that characterizing the formalism. The strongly

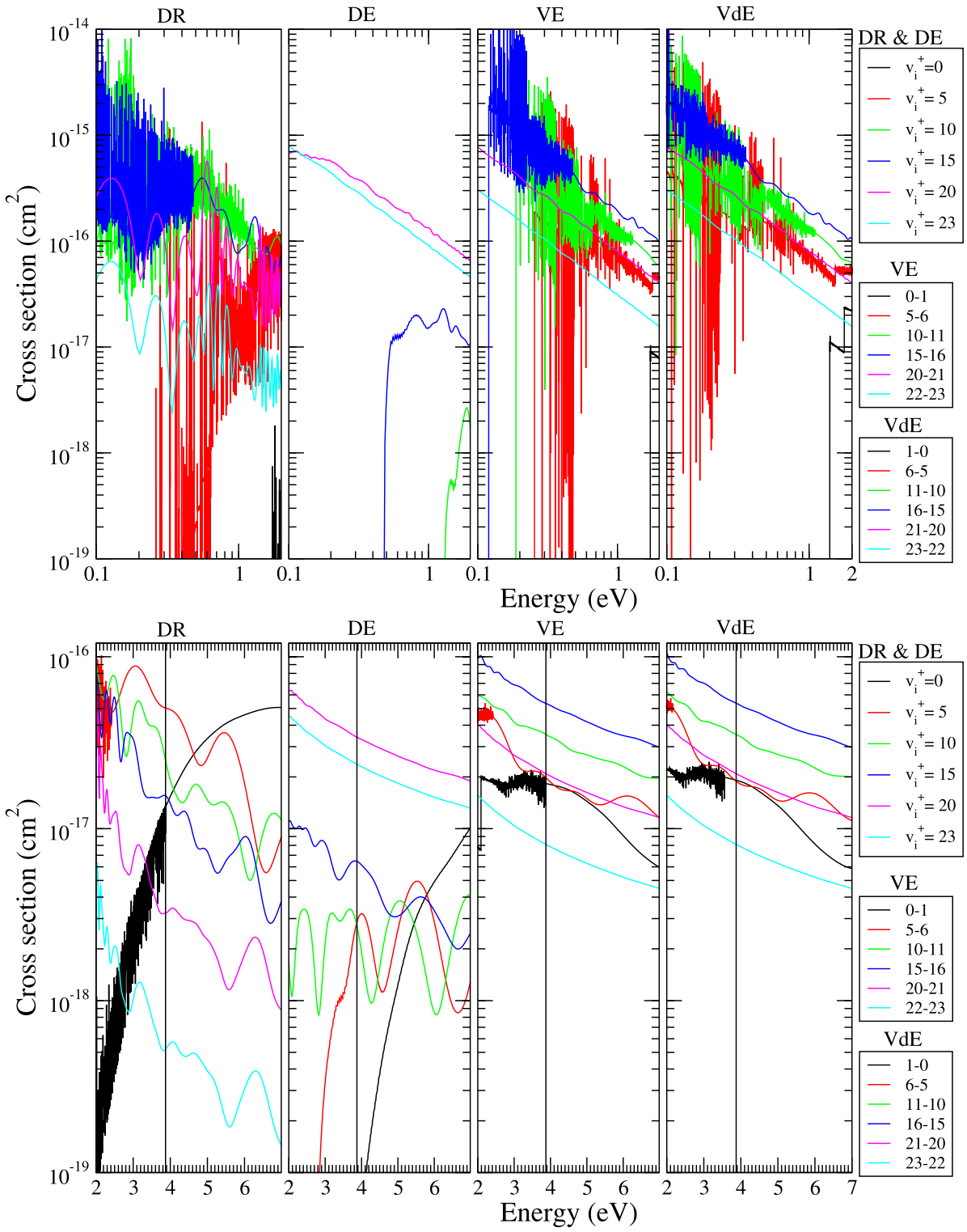

Figure 2. Overview on vibrational-state-resolved electron-ArH^+ cross sections for the dissociative recombination (DR), dissociative excitation (DE), vibrational excitation (VE) and de-excitation (VdE) processes. The vertical lines correspond to the dissociation energy (D_0) of the ion.

nonlinear link between the input structure data and the results of the quantum dynamics modeling makes difficult a global estimation of the accuracy of our cross section and rate coefficients.

5. FITTING of DR and DE rate coefficients

The calculated rate coefficients for DR of ArH^+ in each of its first 24 vibrational states ($v_i^+ = 0 \rightarrow 23$) have been fitted

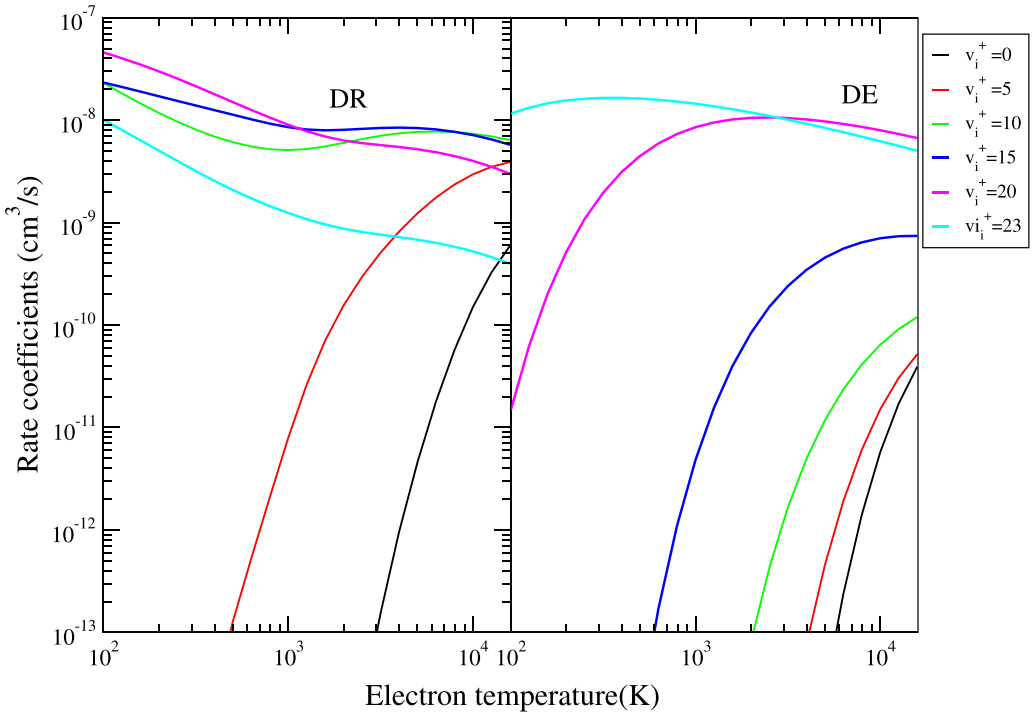

Figure 3. Rate coefficients for dissociative recombination (DR) and the dissociative excitation (DE) processes computed with our MQDT-based method.

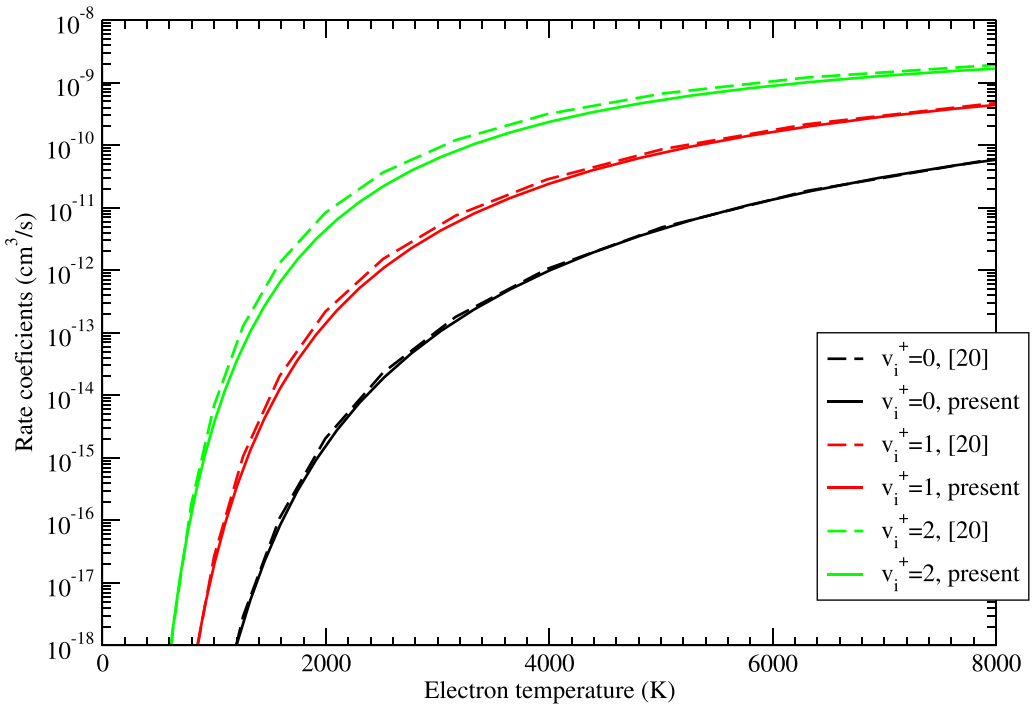

Figure 4. Comparison between the DR rate coefficients for the three lowest vibrationally excited states from the present calculations and the previous ones (Abdoulanziz *et al* [20]).

Table 3. Parameters used in equation (23) for the DR rate coefficients of ArH^+: $v_i^+ = 0$–10.

v_i^+	T_{min}, T_{max}	$A_{v_i^+}$	$\alpha_{v_i^+}$	$B_{v_i^+}$	Relative accuracy
0	100 400	$0.553\,550\,946 \times 10^{-11}$	$0.136\,995\,622 \times 10^{+00}$	$0.199\,882\,496 \times 10^{+05}$	0.0231
0	400 1000	$0.371\,557\,758 \times 10^{-13}$	$0.812\,994\,020 \times 10^{+00}$	$0.196\,002\,081 \times 10^{+05}$	0.0136
0	1000 5000	$0.227\,643\,079 \times 10^{-20}$	$0.292\,810\,828 \times 10^{+01}$	$0.176\,019\,189 \times 10^{+05}$	0.0032
0	5000 15 000	$0.185\,077\,436 \times 10^{-11}$	$0.794\,517\,289 \times 10^{+00}$	$0.294\,108\,753 \times 10^{+05}$	0.0197
1	100 400	$0.110\,856\,185 \times 10^{-09}$	$0.972\,563\,969 \times 10^{-01}$	$0.162\,628\,087 \times 10^{+05}$	0.0241
1	400 1000	$0.693\,730\,597 \times 10^{-12}$	$0.780\,773\,862 \times 10^{+00}$	$0.158\,642\,627 \times 10^{+05}$	0.0147
1	1000 5000	$0.125\,173\,945 \times 10^{-15}$	$0.192\,182\,001 \times 10^{+01}$	$0.151\,173\,526 \times 10^{+05}$	0.0381
1	5000 15 000	$0.138\,065\,234 \times 10^{-07}$	$-0.480\,497\,875 \times 10^{-01}$	$0.240\,781\,864 \times 10^{+05}$	0.0095
2	100 400	$0.819\,631\,090 \times 10^{-09}$	$0.505\,022\,433 \times 10^{-01}$	$0.127\,116\,087 \times 10^{+05}$	0.0248
2	400 1000	$0.294\,484\,358 \times 10^{-11}$	$0.808\,309\,952 \times 10^{+00}$	$0.122\,681\,336 \times 10^{+05}$	0.0169
2	1000 5000	$0.286\,182\,638 \times 10^{-12}$	$0.118\,468\,101 \times 10^{+01}$	$0.125\,220\,429 \times 10^{+05}$	0.0678
2	5000 15 000	$0.303\,737\,808 \times 10^{-05}$	$-0.569\,536\,324 \times 10^{+00}$	$0.190\,696\,403 \times 10^{+05}$	0.0025
3	100 400	$0.220\,977\,740 \times 10^{-08}$	$0.152\,714\,511 \times 10^{-01}$	$0.932\,457\,236 \times 10^{+04}$	0.0260
3	400 1000	$0.182\,190\,673 \times 10^{-11}$	$0.973\,180\,821 \times 10^{+00}$	$0.876\,982\,976 \times 10^{+04}$	0.0211
3	1000 5000	$0.760\,068\,124 \times 10^{-10}$	$0.612\,156\,554 \times 10^{+00}$	$0.998\,813\,696 \times 10^{+04}$	0.0886
3	5000 15 000	$0.166\,920\,046 \times 10^{-04}$	$-0.748\,640\,863 \times 10^{+00}$	$0.139\,443\,512 \times 10^{+05}$	0.0017
4	100 400	$0.205\,178\,052 \times 10^{-08}$	$-0.428\,061\,052 \times 10^{-01}$	$0.610\,419\,639 \times 10^{+04}$	0.0273
4	400 1000	$0.117\,407\,371 \times 10^{-13}$	$0.159\,945\,158 \times 10^{+01}$	$0.519\,622\,135 \times 10^{+04}$	0.0310
4	1000 5000	$0.338\,102\,091 \times 10^{-08}$	$0.148\,940\,147 \times 10^{+00}$	$0.772\,826\,726 \times 10^{+04}$	0.0926
4	5000 15 000	$0.397\,362\,096 \times 10^{-06}$	$-0.406\,537\,725 \times 10^{+00}$	$0.823\,957\,728 \times 10^{+04}$	0.0018
5	100 400	$0.810\,631\,324 \times 10^{-12}$	$0.677\,010\,421 \times 10^{+00}$	$0.302\,435\,547 \times 10^{+04}$	0.0313
5	400 1000	$0.405\,315\,543 \times 10^{-24}$	$0.457\,686\,011 \times 10^{+01}$	$0.101\,211\,702 \times 10^{+04}$	0.0313
5	1000 5000	$0.384\,191\,700 \times 10^{-10}$	$0.528\,051\,427 \times 10^{+00}$	$0.522\,650\,240 \times 10^{+04}$	0.0169
5	5000 15 000	$0.188\,328\,754 \times 10^{-07}$	$-0.987\,148\,562 \times 10^{-01}$	$0.945\,798\,911 \times 10^{+04}$	0.0076
6	100 400	$0.236\,557\,239 \times 10^{-09}$	$0.194\,035\,862 \times 10^{+00}$	$0.114\,390\,845 \times 10^{+03}$	0.0154
6	400 1000	$0.540\,368\,268 \times 10^{-09}$	$0.555\,081\,466 \times 10^{-01}$	$0.109\,012\,288 \times 10^{+03}$	0.0083
6	1000 5000	$0.371\,742\,467 \times 10^{-12}$	$0.101\,578\,254 \times 10^{+01}$	$-0.548\,003\,327 \times 10^{+03}$	0.0393
6	5000 15 000	$0.807\,644\,965 \times 10^{-09}$	$0.193\,749\,112 \times 10^{+00}$	$0.306\,141\,805 \times 10^{+04}$	0.0089
7	100 400	$0.162\,054\,843 \times 10^{-09}$	$0.208\,809\,326 \times 10^{+00}$	$0.650\,939\,818 \times 10^{+02}$	0.1121
7	400 1000	$0.229\,564\,929 \times 10^{-11}$	$0.971\,691\,609 \times 10^{+00}$	$0.222\,227\,715 \times 10^{+03}$	0.0241
7	1000 5000	$0.215\,332\,596 \times 10^{-08}$	$0.433\,258\,853 \times 10^{-01}$	$0.664\,980\,298 \times 10^{+03}$	0.0531
7	5000 15 000	$0.682\,124\,375 \times 10^{-08}$	$-0.859\,990\,446 \times 10^{-02}$	$0.395\,117\,924 \times 10^{+04}$	0.0109
8	100 400	$0.554\,111\,453 \times 10^{-07}$	$-0.336\,746\,996 \times 10^{+00}$	$-0.295\,318\,662 \times 10^{+02}$	0.0052
8	400 1000	$0.103\,096\,576 \times 10^{-06}$	$-0.430\,875\,488 \times 10^{+00}$	$-0.785\,142\,920 \times 10^{+01}$	0.0007
8	1000 5000	$0.317\,939\,670 \times 10^{-09}$	$0.276\,200\,229 \times 10^{+00}$	$-0.898\,820\,315 \times 10^{+03}$	0.0326
8	5000 15 000	$0.206\,892\,847 \times 10^{-07}$	$-0.120\,905\,442 \times 10^{+00}$	$0.292\,375\,022 \times 10^{+04}$	0.0087
9	100 400	$0.579\,323\,775 \times 10^{-07}$	$-0.447\,945\,464 \times 10^{+00}$	$0.499\,834\,972 \times 10^{+02}$	0.0123
9	400 1000	$0.367\,415\,831 \times 10^{-08}$	$-0.768\,742\,328 \times 10^{-01}$	$-0.167\,874\,487 \times 10^{+03}$	0.0079
9	1000 5000	$0.723\,960\,191 \times 10^{-12}$	$0.103\,373\,015 \times 10^{+01}$	$-0.103\,757\,326 \times 10^{+04}$	0.0410
9	5000 15 000	$0.114\,137\,600 \times 10^{-05}$	$-0.509\,184\,498 \times 10^{+00}$	$0.489\,701\,281 \times 10^{+04}$	0.0033
10	100 400	$0.149\,395\,515 \times 10^{-06}$	$-0.537\,584\,611 \times 10^{+00}$	$-0.609\,458\,689 \times 10^{+02}$	0.0138
10	400 1000	$0.211\,857\,991 \times 10^{-09}$	$0.395\,429\,638 \times 10^{+00}$	$-0.449\,074\,298 \times 10^{+03}$	0.0052
10	1000 5000	$0.335\,480\,898 \times 10^{-09}$	$0.367\,030\,746 \times 10^{+00}$	$-0.191\,979\,146 \times 10^{+03}$	0.0286
10	5000 15 000	$0.164\,208\,052 \times 10^{-05}$	$-0.550\,619\,633 \times 10^{+00}$	$0.338\,630\,231 \times 10^{+04}$	0.0027

using a mathematical form based on a modified Arrhenius equation:

$$k^{\mathrm{DR,fit}}_{(\mathrm{ArH}^+),v_i^+}(T_e) = A^{\mathrm{DR}}_{v_i^+} T_e^{\alpha^{\mathrm{DR}}_{v_i^+}} \exp\left[-\frac{B^{\mathrm{DR}}_{v_i^+}}{T_e}\right], \qquad (23)$$

over the electron temperature range $100\,\mathrm{K} \leqslant T_e \leqslant 15\,000\,\mathrm{K}$. The values calculated by equation (23) depart from our calculated values by only a few percent. The parameters $A^{\mathrm{DR}}_{v_i^+}$, $\alpha^{\mathrm{DR}}_{v_i^+}$ and $B^{\mathrm{DR}}_{v_i^+}$ are listed in tables 3 and 4. The tables also give the relative accuracy of the fit with respect to the original data evaluated as the maximum of the ratio $\left|\frac{k^{\mathrm{DR,fit}}_{(\mathrm{ArH}^+),v_i^+} - k_{\mathrm{MQDT}}}{k_{\mathrm{MQDT}}}\right|$ in the stated temperature interval.

By using the same formula in equation (23) for the DR process, we fitted the corresponding rates for the DE process, over the electron temperature range $100\,\mathrm{K} \leqslant T_e \leqslant 15\,000\,\mathrm{K}$. The parameters $A^{\mathrm{DE}}_{v_i^+}$, $\alpha^{\mathrm{DE}}_{v_i^+}$ and $B^{\mathrm{DE}}_{v_i^+}$ are listed in tables 5 and 6. In the table, the relative accuracy of the fitting with respect to the original value is also given.

Table 4. Parameters used in equation (23) for the DR rate coefficients of ArH^+: $v_i^+ = 11$–23.

v_i^+	T_{min}, T_{max}	$A_{v_i^+}$	$\alpha_{v_i^+}$	$B_{v_i^+}$	Relative accuracy
11	100 400	$0.241\,560\,151 \times 10^{-07}$	$-0.124\,357\,859 \times 10^{+00}$	$-0.329\,206\,513 \times 10^{+02}$	0.0076
11	400 1000	$0.135\,845\,516 \times 10^{-07}$	$-0.382\,762\,815 \times 10^{-01}$	$-0.564\,165\,994 \times 10^{+02}$	0.0001
11	1000 5000	$0.283\,326\,432 \times 10^{-07}$	$-0.127\,836\,912 \times 10^{+00}$	$0.592\,386\,721 \times 10^{+02}$	0.0037
11	5000 15 000	$0.150\,173\,044 \times 10^{-05}$	$-0.545\,286\,880 \times 10^{+00}$	$0.216\,944\,260 \times 10^{+04}$	0.0031
12	100 400	$0.755\,548\,884 \times 10^{-07}$	$-0.231\,584\,194 \times 10^{+00}$	$-0.552\,258\,253 \times 10^{+02}$	0.0053
12	400 1000	$0.232\,238\,259 \times 10^{-06}$	$-0.396\,366\,410 \times 10^{+00}$	$-0.184\,371\,809 \times 10^{+01}$	0.0006
12	1000 5000	$0.494\,314\,273 \times 10^{-07}$	$-0.202\,711\,273 \times 10^{+00}$	$-0.210\,738\,857 \times 10^{+03}$	0.0031
12	5000 15 000	$0.124\,890\,007 \times 10^{-05}$	$-0.535\,352\,333 \times 10^{+00}$	$0.177\,078\,104 \times 10^{+04}$	0.0036
13	100 400	$0.462\,670\,160 \times 10^{-07}$	$-0.191\,253\,679 \times 10^{+00}$	$-0.260\,897\,984 \times 10^{-01}$	0.0073
13	400 1000	$0.124\,877\,150 \times 10^{-07}$	$0.586\,461\,230 \times 10^{-02}$	$-0.494\,005\,924 \times 10^{+02}$	0.0027
13	1000 5000	$0.227\,379\,505 \times 10^{-06}$	$-0.367\,243\,877 \times 10^{+00}$	$0.276\,292\,838 \times 10^{+03}$	0.0049
13	5000 15 000	$0.177\,373\,343 \times 10^{-05}$	$-0.574\,140\,662 \times 10^{+00}$	$0.172\,036\,097 \times 10^{+04}$	0.0032
14	100 400	$0.398\,238\,408 \times 10^{-06}$	$-0.467\,500\,149 \times 10^{+00}$	$-0.485\,850\,823 \times 10^{+01}$	0.0068
14	400 1000	$0.116\,436\,502 \times 10^{-05}$	$-0.629\,299\,103 \times 10^{+00}$	$0.348\,446\,447 \times 10^{+02}$	0.0022
14	1000 5000	$0.703\,444\,213 \times 10^{-08}$	$0.141\,446\,029 \times 10^{-01}$	$-0.629\,711\,153 \times 10^{+03}$	0.0045
14	5000 15 000	$0.340\,237\,433 \times 10^{-05}$	$-0.638\,318\,997 \times 10^{+00}$	$0.253\,726\,281 \times 10^{+04}$	0.0033
15	100 400	$0.196\,688\,384 \times 10^{-06}$	$-0.458\,875\,149 \times 10^{+00}$	$0.214\,643\,193 \times 10^{+01}$	0.0018
15	400 1000	$0.424\,437\,919 \times 10^{-07}$	$-0.247\,497\,572 \times 10^{+00}$	$-0.106\,289\,049 \times 10^{+03}$	0.0043
15	1000 5000	$0.130\,661\,029 \times 10^{-08}$	$0.211\,560\,812 \times 10^{+00}$	$-0.420\,772\,588 \times 10^{+03}$	0.0212
15	5000 15 000	$0.739\,601\,646 \times 10^{-05}$	$-0.717\,320\,920 \times 10^{+00}$	$0.338\,054\,405 \times 10^{+04}$	0.0028
16	100 400	$0.967\,668\,045 \times 10^{-07}$	$-0.300\,126\,140 \times 10^{+00}$	$0.489\,835\,375 \times 10^{+01}$	0.0045
16	400 1000	$0.484\,099\,670 \times 10^{-07}$	$-0.214\,552\,693 \times 10^{+00}$	$-0.698\,083\,626 \times 10^{+02}$	0.0047
16	1000 5000	$0.279\,756\,017 \times 10^{-07}$	$-0.123\,755\,899 \times 10^{+00}$	$0.527\,398\,411 \times 10^{+01}$	0.0170
16	5000 15 000	$0.865\,873\,356 \times 10^{-05}$	$-0.737\,705\,759 \times 10^{+00}$	$0.263\,562\,894 \times 10^{+04}$	0.0028
17	100 400	$0.561\,900\,093 \times 10^{-06}$	$-0.568\,477\,582 \times 10^{+00}$	$0.388\,749\,076 \times 10^{+01}$	0.0144
17	400 1000	$0.950\,526\,018 \times 10^{-09}$	$0.353\,652\,239 \times 10^{+00}$	$-0.336\,330\,861 \times 10^{+03}$	0.0032
17	1000 5000	$0.694\,279\,065 \times 10^{-06}$	$-0.480\,508\,209 \times 10^{+00}$	$0.495\,036\,871 \times 10^{+03}$	0.0033
17	5000 15 000	$0.950\,759\,740 \times 10^{-05}$	$-0.751\,278\,490 \times 10^{+00}$	$0.206\,067\,070 \times 10^{+04}$	0.0030
18	100 400	$0.928\,412\,733 \times 10^{-08}$	$0.195\,250\,072 \times 10^{+00}$	$-0.598\,945\,026 \times 10^{+02}$	0.0097
18	400 1000	$0.661\,534\,590 \times 10^{-05}$	$-0.740\,492\,577 \times 10^{+00}$	$0.324\,939\,505 \times 10^{+03}$	0.0029
18	1000 5000	$0.254\,055\,498 \times 10^{-05}$	$-0.633\,436\,367 \times 10^{+00}$	$0.110\,088\,955 \times 10^{+03}$	0.0122
18	5000 15 000	$0.100\,908\,865 \times 10^{-04}$	$-0.763\,998\,807 \times 10^{+00}$	$0.139\,734\,565 \times 10^{+04}$	0.0034
19	100 400	$0.101\,802\,490 \times 10^{-04}$	$-0.925\,541\,406 \times 10^{+00}$	$0.415\,922\,345 \times 10^{+02}$	0.0107
19	400 1000	$0.171\,082\,144 \times 10^{-03}$	$-0.133\,225\,939 \times 10^{+01}$	$0.195\,027\,055 \times 10^{+03}$	0.0011
19	1000 5000	$0.518\,951\,701 \times 10^{-03}$	$-0.147\,270\,613 \times 10^{+01}$	$0.334\,375\,862 \times 10^{+03}$	0.0013
19	5000 15 000	$0.655\,761\,320 \times 10^{-03}$	$-0.149\,826\,608 \times 10^{+01}$	$0.422\,154\,892 \times 10^{+03}$	0.0000
20	100 400	$0.334\,950\,837 \times 10^{-05}$	$-0.859\,381\,439 \times 10^{+00}$	$0.333\,538\,812 \times 10^{+02}$	0.0029
20	400 1000	$0.665\,456\,577 \times 10^{-06}$	$-0.632\,895\,953 \times 10^{+00}$	$-0.708\,680\,209 \times 10^{+02}$	0.0019
20	1000 5000	$0.300\,274\,826 \times 10^{-08}$	$0.485\,175\,407 \times 10^{-01}$	$-0.766\,229\,774 \times 10^{+03}$	0.0097
20	5000 15 000	$0.158\,577\,259 \times 10^{-04}$	$-0.863\,634\,897 \times 10^{+00}$	$0.334\,246\,840 \times 10^{+04}$	0.0033
21	100 400	$0.258\,281\,502 \times 10^{-05}$	$-0.927\,932\,637 \times 10^{+00}$	$0.417\,488\,516 \times 10^{+02}$	0.0027
21	400 1000	$0.200\,170\,365 \times 10^{-06}$	$-0.565\,380\,890 \times 10^{+00}$	$-0.112\,537\,886 \times 10^{+03}$	0.0014
21	1000 5000	$0.541\,915\,554 \times 10^{-08}$	$-0.113\,021\,807 \times 10^{+00}$	$-0.596\,947\,068 \times 10^{+03}$	0.0046
21	5000 15 000	$0.324\,701\,180 \times 10^{-05}$	$-0.786\,674\,483 \times 10^{+00}$	$0.273\,418\,797 \times 10^{+04}$	0.0035
22	100 400	$0.202\,043\,228 \times 10^{-05}$	$-0.995\,329\,500 \times 10^{+00}$	$0.321\,674\,845 \times 10^{+02}$	0.0068
22	400 1000	$0.704\,797\,368 \times 10^{-07}$	$-0.515\,478\,307 \times 10^{+00}$	$-0.159\,832\,992 \times 10^{+03}$	0.0014
22	1000 5000	$0.239\,215\,757 \times 10^{-08}$	$-0.909\,330\,493 \times 10^{-01}$	$-0.610\,503\,735 \times 10^{+03}$	0.0044
22	5000 15 000	$0.179\,949\,910 \times 10^{-05}$	$-0.789\,687\,332 \times 10^{+00}$	$0.279\,598\,351 \times 10^{+04}$	0.0035
23	100 400	$0.717\,148\,420 \times 10^{-06}$	$-0.943\,989\,862 \times 10^{+00}$	$-0.822\,310\,265 \times 10^{+01}$	0.0074
23	400 1000	$0.245\,643\,927 \times 10^{-07}$	$-0.460\,716\,544 \times 10^{+00}$	$-0.199\,202\,446 \times 10^{+03}$	0.0013
23	1000 5000	$0.105\,780\,714 \times 10^{-08}$	$-0.649\,986\,954 \times 10^{-01}$	$-0.611\,358\,065 \times 10^{+03}$	0.0048
23	5000 15 000	$0.107\,223\,040 \times 10^{-05}$	$-0.797\,001\,187 \times 10^{+00}$	$0.288\,106\,799 \times 10^{+04}$	0.0034

Table 5. Parameters used in equation (23) for the DE rate coefficients of ArH^+: $v_i^+ = 0$–13.

v_i^+	T_{min}, T_{max}	$A_{v_i^+}$	$\alpha_{v_i^+}$	$B_{v_i^+}$	Relative accuracy
0	100 400	$0.161\,074\,027 \times 10^{-08}$	$-0.118\,015\,032 \times 10^{+00}$	$-0.653\,584\,678 \times 10^{+03}$	0.0024
0	400 1000	$0.118\,188\,100 \times 10^{-13}$	$0.119\,074\,621 \times 10^{+01}$	$-0.605\,714\,472 \times 10^{+04}$	0.0019
0	1000 5000	$0.207\,687\,221 \times 10^{-05}$	$-0.850\,436\,908 \times 10^{+00}$	$0.501\,004\,680 \times 10^{+04}$	0.0246
0	5000 15 000	$0.547\,553\,158 \times 10^{-03}$	$-0.137\,000\,956 \times 10^{+01}$	$0.185\,160\,964 \times 10^{+05}$	0.0164
1	100 400	$0.375\,699\,154 \times 10^{-13}$	$0.925\,742\,374 \times 10^{+00}$	$0.446\,215\,579 \times 10^{+05}$	0.0041
1	400 1000	$0.531\,358\,744 \times 10^{-20}$	$0.273\,119\,543 \times 10^{+01}$	$0.386\,105\,781 \times 10^{+05}$	0.0004
1	1000 5000	$0.829\,070\,899 \times 10^{-02}$	$-0.143\,469\,510 \times 10^{+01}$	$0.878\,422\,975 \times 10^{+05}$	0.0085
1	5000 15 000	$0.102\,608\,529 \times 10^{-01}$	$-0.151\,442\,683 \times 10^{+01}$	$0.777\,248\,316 \times 10^{+05}$	0.0058
2	100 400	$0.177\,352\,619 \times 10^{-11}$	$0.622\,781\,577 \times 10^{+00}$	$0.411\,272\,422 \times 10^{+05}$	0.0070
2	400 1000	$0.366\,213\,072 \times 10^{-13}$	$0.106\,327\,149 \times 10^{+01}$	$0.396\,002\,151 \times 10^{+05}$	0.0015
2	1000 5000	$0.340\,985\,650 \times 10^{-03}$	$-0.130\,060\,042 \times 10^{+01}$	$0.601\,714\,044 \times 10^{+05}$	0.0302
2	5000 15 000	$0.473\,883\,673 \times 10^{-02}$	$-0.152\,722\,592 \times 10^{+01}$	$0.694\,356\,791 \times 10^{+05}$	0.0277
3	100 400	$0.713\,832\,788 \times 10^{-10}$	$0.113\,686\,227 \times 10^{+00}$	$0.379\,439\,597 \times 10^{+05}$	0.0054
3	400 1000	$0.333\,370\,943 \times 10^{-07}$	$-0.608\,105\,124 \times 10^{+00}$	$0.399\,289\,229 \times 10^{+05}$	0.0041
3	1000 5000	$0.216\,325\,745 \times 10^{-50}$	$0.946\,073\,482 \times 10^{+01}$	$-0.627\,007\,684 \times 10^{+05}$	0.0315
3	5000 15 000	$0.274\,456\,975 \times 10^{+00}$	$-0.183\,315\,105 \times 10^{+01}$	$0.921\,632\,480 \times 10^{+05}$	0.0081
4	100 400	$0.756\,446\,995 \times 10^{-17}$	$0.197\,935\,941 \times 10^{+01}$	$0.330\,532\,178 \times 10^{+05}$	0.0066
4	400 1000	$0.119\,498\,545 \times 10^{-10}$	$0.427\,441\,209 \times 10^{+00}$	$0.404\,226\,611 \times 10^{+05}$	0.0017
4	1000 5000	$0.249\,438\,298 \times 10^{-12}$	$0.743\,822\,791 \times 10^{+00}$	$0.315\,333\,861 \times 10^{+05}$	0.0433
4	5000 15 000	$0.803\,555\,726 \times 10^{-04}$	$-0.113\,898\,610 \times 10^{+01}$	$0.480\,759\,994 \times 10^{+05}$	0.0198
5	100 400	$0.300\,321\,184 \times 10^{-10}$	$0.211\,241\,145 \times 10^{+00}$	$0.313\,084\,507 \times 10^{+05}$	0.0171
5	400 1000	$0.344\,656\,024 \times 10^{-06}$	$-0.878\,311\,647 \times 10^{+00}$	$0.344\,850\,317 \times 10^{+05}$	0.0093
5	1000 5000	$0.718\,488\,480 \times 10^{-25}$	$0.376\,081\,905 \times 10^{+01}$	$0.154\,763\,520 \times 10^{+05}$	0.0571
5	5000 15 000	$0.153\,839\,291 \times 10^{-01}$	$-0.159\,079\,053 \times 10^{+01}$	$0.738\,959\,711 \times 10^{+05}$	0.0081
6	100 400	$0.758\,273\,760 \times 10^{-08}$	$-0.825\,822\,875 \times 10^{+00}$	$0.285\,854\,727 \times 10^{+05}$	0.0163
6	400 1000	$0.121\,206\,951 \times 10^{-61}$	$0.135\,208\,805 \times 10^{+02}$	$-0.141\,066\,453 \times 10^{+05}$	0.0055
6	1000 5000	$0.136\,465\,697 \times 10^{-10}$	$0.362\,123\,861 \times 10^{+00}$	$0.310\,003\,428 \times 10^{+05}$	0.0343
6	5000 15 000	$0.290\,269\,616 \times 10^{-02}$	$-0.146\,540\,190 \times 10^{+01}$	$0.617\,974\,738 \times 10^{+05}$	0.0071
7	100 400	$0.595\,809\,226 \times 10^{-13}$	$0.101\,340\,264 \times 10^{+01}$	$0.256\,614\,573 \times 10^{+05}$	0.0109
7	400 1000	$0.351\,131\,194 \times 10^{-10}$	$0.126\,788\,166 \times 10^{+00}$	$0.246\,976\,082 \times 10^{+05}$	0.0008
7	1000 5000	$0.201\,849\,195 \times 10^{+11}$	$-0.438\,557\,041 \times 10^{+01}$	$0.952\,672\,549 \times 10^{+05}$	0.0182
7	5000 15 000	$0.105\,499\,213 \times 10^{-01}$	$-0.157\,647\,176 \times 10^{+01}$	$0.656\,559,991 \times 10^{+05}$	0.0046
8	100 400	$0.183\,432\,272 \times 10^{-09}$	$-0.114\,347\,745 \times 10^{+00}$	$0.230\,182\,161 \times 10^{+05}$	0.0169
8	400 1000	$0.110\,908\,452 \times 10^{-28}$	$0.493\,026\,710 \times 10^{+01}$	$0.572\,372\,833 \times 10^{+04}$	0.0033
8	1000 5000	$0.302\,704\,277 \times 10^{-14}$	$0.113\,955\,842 \times 10^{+01}$	$0.839\,416\,412 \times 10^{+04}$	0.0265
8	5000 15 000	$0.543\,749\,213 \times 10^{-01}$	$-0.171\,360\,900 \times 10^{+01}$	$0.749\,314\,001 \times 10^{+05}$	0.0026
9	100 400	$0.158\,481\,665 \times 10^{-07}$	$-0.730\,050\,400 \times 10^{+00}$	$0.203\,420\,603 \times 10^{+05}$	0.0407
9	400 1000	$0.171\,335\,299 \times 10^{-37}$	$0.718\,002\,550 \times 10^{+01}$	$-0.581\,195\,026 \times 10^{+04}$	0.0089
9	1000 5000	$0.263\,302\,819 \times 10^{-14}$	$0.113\,272\,818 \times 10^{+01}$	$0.252\,546\,833 \times 10^{+04}$	0.0102
9	5000 15 000	$0.587\,690\,667 \times 10^{+00}$	$-0.190\,883\,852 \times 10^{+01}$	$0.890\,590\,746 \times 10^{+05}$	0.0028
10	100 400	$0.137\,931\,823 \times 10^{-09}$	$0.162\,474\,178 \times 10^{+00}$	$0.201\,285\,466 \times 10^{+05}$	0.0107
10	400 1000	$0.280\,583\,550 \times 10^{-11}$	$0.540\,636\,502 \times 10^{+00}$	$0.184\,154\,741 \times 10^{+05}$	0.0046
10	1000 5000	$0.904\,580\,832 \times 10^{-09}$	$-0.840\,957\,096 \times 10^{-01}$	$0.229\,718\,569 \times 10^{+05}$	0.0188
10	5000 15 000	$0.167\,449\,436 \times 10^{+01}$	$-0.199\,195\,003 \times 10^{+01}$	$0.953\,320\,036 \times 10^{+05}$	0.0023
11	100 400	$0.240\,861\,133 \times 10^{-09}$	$-0.954\,607\,857 \times 10^{-01}$	$0.152\,165\,200 \times 10^{+05}$	0.0047
11	400 1000	$0.797\,900\,557 \times 10^{-04}$	$-0.130\,089\,518 \times 10^{+01}$	$0.258\,005\,748 \times 10^{+05}$	0.0050
11	1000 5000	$0.762\,878\,059 \times 10^{-10}$	$0.152\,158\,589 \times 10^{+00}$	$0.152\,957\,687 \times 10^{+05}$	0.0043
11	5000 15 000	$0.180\,281\,488 \times 10^{+01}$	$-0.198\,903\,358 \times 10^{+01}$	$0.953\,699\,264 \times 10^{+05}$	0.0013
12	100 400	$0.393\,345\,385 \times 10^{-11}$	$0.636\,374\,487 \times 10^{+00}$	$0.132\,205\,797 \times 10^{+05}$	0.0033
12	400 1000	$0.234\,078\,899 \times 10^{-08}$	$-0.230\,923\,937 \times 10^{+00}$	$0.128\,342\,527 \times 10^{+05}$	0.0008
12	1000 5000	$0.400\,450\,674 \times 10^{-08}$	$-0.232\,108\,616 \times 10^{+00}$	$0.167\,777\,278 \times 10^{+05}$	0.0092
12	5000 15 000	$0.224\,127\,664 \times 10^{+01}$	$-0.200\,008\,050 \times 10^{+01}$	$0.951\,463\,785 \times 10^{+05}$	0.0010
13	100 400	$0.778\,955\,016 \times 10^{-14}$	$0.137\,660\,634 \times 10^{+01}$	$0.951\,612\,479 \times 10^{+04}$	0.0094
13	400 1000	$0.539\,294\,341 \times 10^{-07}$	$-0.542\,167\,082 \times 10^{+00}$	$0.126\,521\,066 \times 10^{+05}$	0.0018
13	1000 5000	$0.794\,510\,725 \times 10^{-09}$	$-0.711\,963\,436 \times 10^{-01}$	$0.110\,644\,399 \times 10^{+05}$	0.0021
13	5000 15 000	$0.744\,394\,557 \times 10^{+00}$	$-0.190\,185\,560 \times 10^{+01}$	$0.867\,181\,723 \times 10^{+05}$	0.0012

Table 6. Parameters used in equation (23) for the DE rate coefficients of ArH^+: $v_i^+ = 14$–23.

v_i^+	T_{min}, T_{max}	$A_{v_i^+}$	$\alpha_{v_i^+}$	$B_{v_i^+}$	Relative accuracy
14	100 400	$0.519\,353\,858 \times 10^{-08}$	$-0.249\,191\,171 \times 10^{+00}$	$0.950\,844\,029 \times 10^{+04}$	0.0033
14	400 1000	$0.166\,504\,203 \times 10^{-10}$	$0.392\,913\,484 \times 10^{+00}$	$0.713\,932\,842 \times 10^{+04}$	0.0037
14	1000 5000	$0.171\,140\,629 \times 10^{-08}$	$-0.128\,377\,022 \times 10^{+00}$	$0.805\,741\,805 \times 10^{+04}$	0.0021
14	5000 15 000	$0.127\,074\,983 \times 10^{+00}$	$-0.174\,044\,608 \times 10^{+01}$	$0.724\,873\,333 \times 10^{+05}$	0.0016
15	100 400	$0.468\,833\,613 \times 10^{-06}$	$-0.732\,409\,571 \times 10^{+00}$	$0.881\,276\,914 \times 10^{+04}$	0.0139
15	400 1000	$0.206\,671\,029 \times 10^{-09}$	$0.165\,532\,323 \times 10^{+00}$	$0.616\,672\,195 \times 10^{+04}$	0.0006
15	1000 5000	$0.258\,218\,589 \times 10^{-07}$	$-0.354\,656\,824 \times 10^{+00}$	$0.877\,588\,652 \times 10^{+04}$	0.0065
15	5000 15 000	$0.229\,680\,020 \times 10^{-01}$	$-0.157\,598\,698 \times 10^{+01}$	$0.573\,441\,177 \times 10^{+05}$	0.0018
16	100 400	$0.181\,595\,141 \times 10^{-09}$	$0.252\,685\,671 \times 10^{+00}$	$0.527\,550\,016 \times 10^{+04}$	0.0062
16	400 1000	$0.979\,707\,258 \times 10^{-09}$	$0.455\,298\,848 \times 10^{-01}$	$0.549\,332\,623 \times 10^{+04}$	0.0003
16	1000 5000	$0.284\,967\,681 \times 10^{-06}$	$-0.554\,526\,078 \times 10^{+00}$	$0.938\,296\,755 \times 10^{+04}$	0.0126
16	5000 15 000	$0.850\,136\,474 \times 10^{-02}$	$-0.147\,016\,427 \times 10^{+01}$	$0.473\,970\,452 \times 10^{+05}$	0.0016
17	100 400	$0.402\,085\,545 \times 10^{-10}$	$0.469\,372\,175 \times 10^{+00}$	$0.404\,785\,775 \times 10^{+04}$	0.0058
17	400 1000	$0.515\,885\,463 \times 10^{-08}$	$-0.964\,057\,764 \times 10^{-01}$	$0.564\,216\,018 \times 10^{+04}$	0.0000
17	1000 5000	$0.692\,053\,503 \times 10^{-06}$	$-0.622\,722\,997 \times 10^{+00}$	$0.859\,797\,375 \times 10^{+04}$	0.0077
17	5000 15 000	$0.585\,661\,335 \times 10^{-02}$	$-0.142\,227\,537 \times 10^{+01}$	$0.436\,007\,430 \times 10^{+05}$	0.0012
18	100 400	$0.139\,954\,785 \times 10^{-08}$	$0.780\,832\,579 \times 10^{-01}$	$0.298\,877\,707 \times 10^{+04}$	0.0140
18	400 1000	$0.242\,114\,494 \times 10^{-08}$	$0.874\,441\,576 \times 10^{-02}$	$0.312\,821\,780 \times 10^{+04}$	0.0005
18	1000 5000	$0.737\,490\,621 \times 10^{-06}$	$-0.606\,836\,864 \times 10^{+00}$	$0.651\,907\,993 \times 10^{+04}$	0.0031
18	5000 15 000	$0.686\,186\,977 \times 10^{-02}$	$-0.140\,989\,228 \times 10^{+01}$	$0.435\,479\,524 \times 10^{+05}$	0.0008
19	100 400	$0.394\,932\,834 \times 10^{-07}$	$-0.257\,123\,888 \times 10^{+00}$	$0.219\,417\,434 \times 10^{+04}$	0.0062
19	400 1000	$0.184\,926\,939 \times 10^{-07}$	$-0.170\,864\,213 \times 10^{+00}$	$0.191\,773\,949 \times 10^{+04}$	0.0012
19	1000 5000	$0.509\,707\,623 \times 10^{-06}$	$-0.527\,186\,875 \times 10^{+00}$	$0.394\,852\,857 \times 10^{+04}$	0.0020
19	5000 15 000	$0.122\,745\,023 \times 10^{-01}$	$-0.141\,372\,831 \times 10^{+01}$	$0.449\,140\,446 \times 10^{+05}$	0.0006
20	100 400	$0.314\,287\,026 \times 10^{-06}$	$-0.430\,461\,213 \times 10^{+00}$	$0.171\,483\,171 \times 10^{+04}$	0.0074
20	400 1000	$0.188\,930\,725 \times 10^{-06}$	$-0.368\,921\,345 \times 10^{+00}$	$0.159\,611\,662 \times 10^{+04}$	0.0010
20	1000 5000	$0.557\,384\,538 \times 10^{-06}$	$-0.483\,304\,144 \times 10^{+00}$	$0.238\,176\,771 \times 10^{+04}$	0.0017
20	5000 15 000	$0.225\,884\,800 \times 10^{-01}$	$-0.141\,587\,873 \times 10^{+01}$	$0.453\,692\,769 \times 10^{+05}$	0.0005
21	100 400	$0.314\,450\,726 \times 10^{-06}$	$-0.377\,658\,370 \times 10^{+00}$	$0.104\,861\,956 \times 10^{+04}$	0.0087
21	400 1000	$0.427\,899\,047 \times 10^{-06}$	$-0.419\,458\,604 \times 10^{+00}$	$0.103\,574\,612 \times 10^{+04}$	0.0010
21	1000 5000	$0.798\,329\,840 \times 10^{-06}$	$-0.484\,025\,844 \times 10^{+00}$	$0.156\,872\,280 \times 10^{+04}$	0.0019
21	5000 15 000	$0.258\,334\,763 \times 10^{-01}$	$-0.139\,662\,225 \times 10^{+01}$	$0.437\,819\,483 \times 10^{+05}$	0.0005
22	100 400	$0.247\,371\,422 \times 10^{-06}$	$-0.354\,442\,925 \times 10^{+00}$	$0.667\,939\,762 \times 10^{+03}$	0.0056
22	400 1000	$0.564\,367\,941 \times 10^{-06}$	$-0.456\,796\,692 \times 10^{+00}$	$0.822\,491\,600 \times 10^{+03}$	0.0008
22	1000 5000	$0.741\,600\,118 \times 10^{-06}$	$-0.484\,615\,849 \times 10^{+00}$	$0.108\,558\,342 \times 10^{+04}$	0.0019
22	5000 15 000	$0.215\,627\,335 \times 10^{-01}$	$-0.138\,772\,003 \times 10^{+01}$	$0.429\,231\,955 \times 10^{+05}$	0.0004
23	100 400	$0.191\,419\,429 \times 10^{-06}$	$-0.352\,741\,602 \times 10^{+00}$	$0.419\,299\,389 \times 10^{+03}$	0.0013
23	400 1000	$0.500\,770\,945 \times 10^{-06}$	$-0.470\,223\,147 \times 10^{+00}$	$0.636\,023\,850 \times 10^{+03}$	0.0004
23	1000 5000	$0.587\,347\,786 \times 10^{-06}$	$-0.486\,504\,706 \times 10^{+00}$	$0.787\,755\,489 \times 10^{+03}$	0.0014
23	5000 15 000	$0.151\,600\,162 \times 10^{-01}$	$-0.137\,899\,351 \times 10^{+01}$	$0.422\,135\,272 \times 10^{+05}$	0.0004

6. Conclusions

In the present work, we presented a theoretical study of vibrationally-resolved cross sections and the corresponding rate coefficients for electron collisions with the ArH^+ molecular ion calculated in the framework of the MQDT approach. In particular, we considered electron energies up to 7 eV, and all the vibrational levels of the ion, taking into account simultaneously all the four competitive processes of DR, VE, VdE and DE.

These calculations were motivated by the need of supplying data for kinetic modeling of plasmas containing ArH^+ molecular ions for which high non-equilibrium effects are not negligible and electron-vibration energy exchange are very important to explain relaxation of the plasma, as shown in the papers Laporta *et al*, Heritier *et al* [41, 42] and Laporta *et al* [43] for the case of oxygen, nitrogen and deuterium.

Thus, fitting parameters for the vibrationally-resolved rate constants based on a modified Arrhenius law have been provided for electron temperature ranging from 100 K to 15 000 K.

Validation of these data is a tricky task but may be possible under specific conditions. For this the electron energy distribution must be Maxwellian, the temperature must be high enough to lead to sufficiently high VE, but at the same time low enough to avoid strong dissociation of the molecular ion. The use of

a thermal arc device implemented in Ar–H_2 mixtures at atmospheric pressure could be appropriate. If the plasma is in equilibrium, the kinetic aspects do not play a role. The arc should therefore be out of equilibrium: the only way to satisfy these different and contradictory conditions is to study the unstable behavior of an arc plasma with ArH^+ as the main ion during its extinction and particularly to follow temperature levels lower than 6000 K.

The present results are not resolved with respect to the rotational structure of the ion target. This was the case also for the measurements of Mitchell *et al* in 2005 [15]. A new generation of electrostatic storage rings is nowadays available, capable of very precise rotationally resolved measurements. This will allow further more accurate studies of electron/ArH^+ collisions in the near future at CSR in Heidelberg [44] or at DESIREE in Stockholm [45].

Data availability statement

All data that support the findings of this study are included within the article (and any supplementary files).

Acknowledgments

I F S and V L acknowledge the Programme National 'Physique et Chimie du Milieu Interstellaire' (PCMI) of CNRS/INSU with INC/INP co-funded by CEA and CNES. They also thank for generous financial support from La Région Haute-Normandie via the GRR Electronique, Energie et Matériaux, from the 'Fédération de Recherche Energie, Propulsion, Environnement', and from the LabEx EMC^3 and FEDER via the projects PicoLIBS (ANR-10-LABEX-09-01), EMoPlaF, PTOLEMEE and CO_2-VIRIDIS. I F S thanks for support the International Atomic Energy Agency, Vienna (IAEA), the French 'Agence Nationale pour la Recherche' via the project MONA (ANR-18-CE30-0016), Fédération de Recherche 'Fusion par Confinement Magnétique' (FR-FCM), Groupement de Recherche 'Etude des Milieux Ionisés :Plasmas froids créés par décharge et laser' (GdR-EMILI), and Dr J Zs Mezei for his help in the data processing.

ORCID iDs

A Bultel https://orcid.org/0000-0003-4792-9995
J Tennyson https://orcid.org/0000-0002-4994-5238
I F Schneider https://orcid.org/0000-0002-4379-1768
V Laporta https://orcid.org/0000-0003-4251-407X

References

[1] Voitsenya V, Naidenkova D, Masuzaki S, Kubota Y, Sagara A and Yamazaki K 2006 *J. Plasma Fusion Res. Ser.* **7** 114
[2] Voitsenya V, Naidenkova D, Kubota Y, Masuzaki S, Sagara A and Yarnazaki K 2004 NFS series (NIFS-799) *Research Report* (Tokyo, Japan)
[3] Jimenez-Redondo M, Cueto M, Domenech J L, Tanarro I and Herrero V J 2014 *RSC Adv.* **4** 62030
[4] Sode M, Schwarz-Selinger T and Jacob W 2013 *J. Appl. Phys.* **114** 063302
[5] Kajita M and Kimura N 2020 *J. Phys. B: At. Mol. Opt. Phys.* **53** 135401
[6] Maltsev M, Morozov I and Osina E 2019 *High Temp.* **57** 335
[7] Barlow M *et al* 2013 *Science* **342** 1343
[8] Schilke P *et al* 2014 *A & A* **566** A29
[9] Phelps A V 1992 *J. Phys. Chem. Ref. Data* **21** 883
[10] Rat V, André P and Aubreton J 2002 *Plasma Chem. Plasma Proc.* **22** 475
[11] Bogaerts A and Gijbels R 2000 *J. Anal. At. Spectrom.* **15** 441
[12] Carrington A and McNab I 1989 *Acc. Chem. Res.* **22** 218
[13] Burm K T A L, Jodoin B, Proulx P and Boulos M I 2003 *Plasma Sources Sci. Technol.* **12** 362
[14] Meulenbroeks R F G, Engeln R A H, Box C, de Bari I, van de Sanden M C M, van der Mullen J A M and Schram D C 1995 *Phys. Plasmas* **2** 1002
[15] Mitchell J B A, Novotny O, LeGarrec J L, Florescu-Mitchell A, Rebrion-Rowe C, Stolyarov A V, Child M S, Svendsen A, Ghazaly M A E and Andersen L H 2005 *J. Phys. B: At. Mol. Opt. Phys.* **38** L175
[16] Dagdigian P J 2018 *Mon. Not. R. Astron. Soc.* **477** 802
[17] Garcia-Vazquez R M, Marquez-Mijarez M, Rubayo-Soneira J and Denis-Alpizar O 2019 VizieR Online Data Catalog J/A+A/631/A86
[18] Stolyarov A V and Child M S 2005 *Phys. Chem. Chem. Phys.* **7** 2259
[19] Dagdigian P J 2018 *Mon. Not. R. Astron. Soc.* **477** 802
[20] Abdoulanziz A, Colboc F, Little D A, Moulane Y, Mezei J Z, Roueff E, Tennyson J, Schneider I F and Laporta V 2018 *Mon. Not. R. Astron. Soc.* **479** 2415
[21] Giusti A 1980 *J. Phys. B: At. Mol. Phys.* **13** 3867
[22] Motapon O, Fifirig M, Florescu A, Tamo F O W, Crumeyrolle O, Varin-Bréant G, Bultel A, Vervisch P, Tennyson J and Schneider I F 2006 *Plasma Sources Sci. Technol.* **15** 23
[23] Tennyson J 2010 *Phys. Rep.* **491** 29
[24] Carr J M, Galiatsatos P G, Gorfinkiel J D, Harvey A G, Lysaght M A, Madden D, Masin Z, Plummer M, Tennyson J and Varambhia H N 2012 *Eur. Phys. J.* D **66** 58
[25] Larsson M and Orel A 2008 *Dissociative Recombination of Molecular Ions* (Cambridge: Cambridge University Press) pp 1–380
[26] Strömholm C *et al* 1995 *Phys. Rev.* A **52** R4320
[27] Teschl G 2014 *Graduate Studies in Mathematics* vol 157 (Providence, RI: American Mathematical Society)
[28] Hotop H, Roth T E, Ruf M-W and Yencha A J 1998 *Theor. Chem. Acc.* **100** 36
[29] Guberman S L and Giusti-Suzor A 1991 *J. Chem. Phys.* **95** 2602
[30] Schneider I F, Dulieu O and Giusti-Suzor A 1991 *J. Phys. B: At. Mol. Opt. Phys.* **24** L289
[31] Takagi H, Kosugi N and Dourneuf M L 1991 *J. Phys. B: At. Mol. Opt. Phys.* **24** 711
[32] Schneider I F, Strömholm C, Carata L, Urbain X, Larsson M and Suzor-Weiner A 1997 *J. Phys. B: At. Mol. Opt. Phys.* **30** 2687
[33] Motapon O, Pop N, Argoubi F, Mezei J Z, Epee M D E, Faure A, Telmini M, Tennyson J and Schneider I F 2014 *Phys. Rev.* A **90** 012706
[34] Little D A, Chakrabarti K, Mezei J Z, Schneider I F and Tennyson J 2014 *Phys. Rev.* A **90** 052705
[35] Mezei Z J, Chakrabarti K, Epée Epée M D, Motapon O, Yuen C H, Ayouz M A, Douguet N, Fonseca dos Santos S, Kokoouline V and Schneider I F 2019 *ACS Earth Space Chem.* **3** 2376
[36] Mezei J Z *et al* 2016 *Plasma Sources Sci. Technol.* **25** 055022

[37] Moulane Y, Mezei J Z, Laporta V, Jehin E, Benkhaldoun Z and Schneider I F 2018 *A & A* **615** A53
[38] Chakrabarti K, Mezei J Z, Motapon O, Faure A, Dulieu O, Hassouni K and Schneider I F 2018 *J. Phys. B: At. Mol. Opt. Phys.* **51** 104002
[39] Motapon O *et al* 2011 *J. Phys.: Conf. Ser.* **300** 012018
[40] Chakrabarti K, Backodissa-Kiminou D R, Pop N, Mezei J Z, Motapon O, Lique F, Dulieu O, Wolf A and Schneider I F 2013 *Phys. Rev.* A **87** 022702
[41] Laporta V, Heritier K and Panesi M 2016 *Chem. Phys.* **472** 44
[42] Heritier K L, Jaffe R L, Laporta V and Panesi M 2014 *J. Chem. Phys.* **141** 184302
[43] Laporta V, Agnello R, Fubiani G, Furno I, Hill C, Reiter D and Taccogna F 2021 *Plasma Phys. Contr. Fus.* **63** 085006
[44] Kalosi A *et al* 2022 *Phys. Rev. Lett.* **128** 183402
[45] Poline M *et al* 2022 *Phys. Rev.* A **106** 012812